

Existence of an upper limit on the density of excitons in carbon nanotubes by diffusion-limited exciton-exciton annihilation: Experiment and theory

Yoichi Murakami^{1,2,*} and Junichiro Kono¹

¹*Department of Electrical and Computer Engineering, Rice University, Houston, Texas 77005, USA*

²*Department of Chemical System Engineering, University of Tokyo, Bunkyo-ku, Tokyo 113-8656, Japan*

(Dated: October 23, 2018)

Through an investigation of photoemission properties of highly-photoexcited single-walled carbon nanotubes, we demonstrate that there is an upper limit on the achievable excitonic density. As the intensity of optical excitation increases, all photoluminescence emission peaks arising from different chirality single-walled carbon nanotubes showed clear saturation in intensity. Each peak exhibited a saturation value that was independent of the excitation wavelength, indicating that there is an upper limit on the excitonic density for each nanotube species. We propose that this saturation behavior is a result of efficient exciton-exciton annihilation through which excitons decay non-radiatively. In order to explain the experimental results and obtain excitonic densities in the saturation regime, we have developed a model, taking into account the generation, diffusion-limited exciton-exciton annihilation, and spontaneous decays of one-dimensional excitons. Using the model, we were able to reproduce the experimentally obtained saturation curves under certain approximations, from which the excitonic densities were estimated. The validity of the model was confirmed through comparison with Monte Carlo simulations. Finally, we show that the conventional rate equation for exciton-exciton annihilation without taking into account exciton diffusion fails to fit the experimentally observed saturation behavior, especially at high excitonic densities.

PACS numbers: 78.67.Ch,71.35.-y,78.55.-m

I. INTRODUCTION

The optical and electronic properties of low-dimensional materials have been an important subject of study in the field of condensed matter physics. In particular, one-dimensional (1-D) materials are predicted to possess unique properties that are distinctly different from those at higher dimensions,^{1,2} primarily due to the enhanced Coulomb interactions among the quantum confined charge carriers. One common feature of optically-excited low-dimensional systems is the formation of strongly bound electron-hole ($e-h$) pairs, or excitons,³ which dominate interband optical spectra. 1-D semiconductors are expected to show an almost complete suppression of optical absorption at the band edges, with a significant fraction of the total oscillator strength taken by the lowest excitonic state.^{4,5}

Early reports of lasing from semiconductor quantum wires (QWRs)^{6,7} invoked much interest in the physics of *high density* 1-D excitons. A number of studies have thus far been performed on such QWR systems during the last two decades to understand many-body phenomena (e.g., lasing, band-gap renormalization, biexciton formation, and the Mott transition),^{8,9,10,11,12,13,14,15} but many aspects are still under debate and not well understood. More recently, studies on high-density $e-h$ pairs have been extended to novel 1-D materials such as conjugated polymers^{16,17,18,19} and single-walled carbon nanotubes (SWNTs).^{20,21,22} The latter are tubular materials made of sp^2 -bonded carbon atoms,²³ attracting much recent interest from diverse research fields due to their unique properties.²⁴ Semiconducting SWNTs are known to have extremely strong quantum confinement

of ~ 1 nm, giving rise to large exciton binding energies on the order of 0.5-1 eV,^{25,26,27} much larger than those of GaAs QWRs (~ 20 meV)^{5,7} and comparable to or larger than those of conjugated polymers (~ 0.4 eV¹⁹ and < 0.1 eV²⁸).

Here, we report results of experimental and theoretical investigations on the properties of photoluminescence (PL) from excitons in SWNTs through nonlinear photoluminescence excitation (PLE) spectroscopy using intense optical pulses. From the clear saturation behavior observed in the intensities of all the PL features as a function of excitation laser intensity as well as the complete *flattening* of the PLE spectra observed at very high laser intensities, we show the existence of an upper limit on the density of excitons that can be accommodated in SWNTs. Such an upper limit is considered to be caused by the diffusive motion of the excitons^{29,30,31} combined with highly rapid and efficient exciton-exciton annihilation (EEA) in SWNTs.²² As described in Section III, we have developed a theoretical model for describing diffusion-limited EEA processes in 1-D, which enabled us to simulate the PL saturation curves and estimate the densities of excitons in SWNTs as a function of excitation intensity.

A portion of this work was described in our earlier letter.³² The purpose of the present paper is to provide a complete description of both experimental and theoretical aspects of this study.

II. EXPERIMENT

A. Experimental methods

The sample was prepared by ultrasonically dispersing CoMoCAT SWNTs in D_2O with 1 wt% sodium cholate for 1 hour, followed by ultracentrifugation at 111,000 g for 4 hours. This centrifugation condition is sufficient to remove SWNT bundles effectively.³³ Only the upper 50 % of the supernatant was collected and used for the experiment. The solution was put in a 1-mm-thick quartz cuvette. The optical density of the sample around the E_{22} resonance was below 0.2, which helped avoid non-uniform excitation and re-absorption of the emitted PL within the sample. The excitation source was an optical parametric amplifier (OPA), producing ~ 250 fs pulses at a repetition rate of 1 kHz, tunable in the visible and near-infrared ranges, pumped by a chirped-pulse amplifier (Clark-MXR, Inc., CPA-2010). Optical filters were carefully selected and set in the beam path to thoroughly eliminate any parasitic wavelength components (mostly in the ultraviolet and near-infrared regions) contained in the OPA beam. The OPA beam was focused onto the sample to a spot size of 300-400 μm . Only the central ~ 2 mm portion of the OPA beam profile (~ 6 mm) was taken out by using an aperture just before the focus to enhance the spot uniformity at the sample. The PL from the sample was focused onto the monochromator entrance and recorded with a liquid-nitrogen-cooled InGaAs 1-D array detector. The obtained PL spectra were corrected for the wavelength-dependence of the grating efficiency and detector sensitivity.

For the data shown in Fig. 1(c), a different sample as well as a different excitation light source was used for verifying the universality of the phenomena observed. In this case, the sample was a dried film of CoMoCAT SWNTs embedded in ι -carrageenan, formed by drying a mixed gel of ι -carrageenan and the centrifuged supernatant of CoMoCAT SWNTs on the surface of a sapphire substrate. The sapphire substrate served as a mechanical support as well as a heat sink of the film during the measurements. The excitation light was 1 kHz and ~ 250 fs optical pulses with a central wavelength of 653 nm (FWHM = 10 nm), produced by filtering whitelight pulses generated by focusing the CPA beam onto a sapphire crystal.

B. Experimental results

Figure 1(a) compares two PL spectra. The black solid curve was obtained using the OPA with a wavelength of 654 nm (or 1.90 eV) and a pulse energy of 29 nJ, while the red dotted curve was obtained using a weak (100 μW) CW laser with a wavelength of 658 nm (or 1.88 eV). It is seen that the relative intensities of different PL peaks are drastically different between the two curves. The inset confirms that the two spectra coincide accurately when the OPA pulse energy was kept very low (300 pJ). Fig-

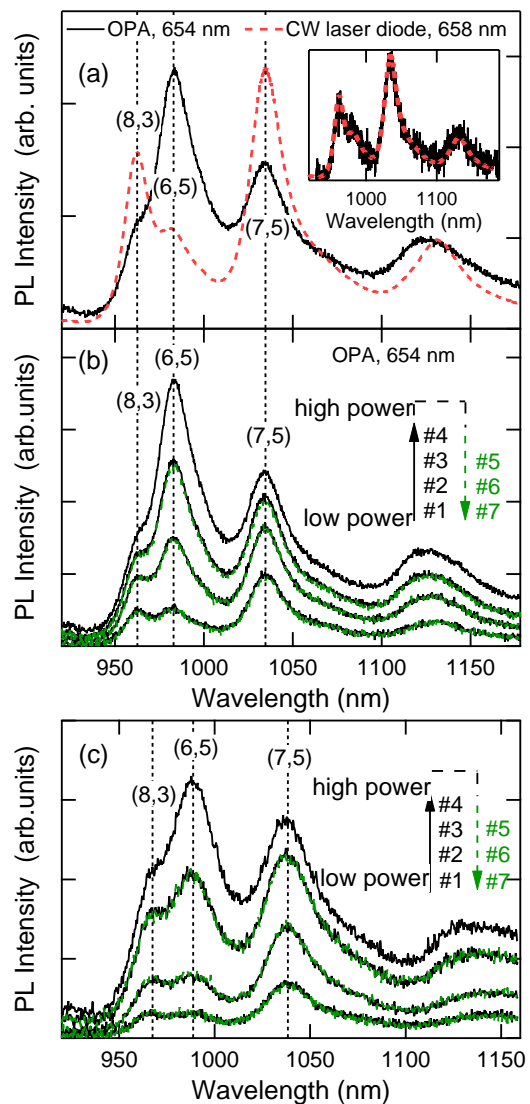


FIG. 1: (color online) Pump-intensity-dependent PL spectra measured for (a, b) the centrifuged supernatant of CoMoCAT SWNTs dispersed in D_2O and (c) CoMoCAT SWNTs embedded in a dried ι -carrageenan film: (a) Black solid — spectrum obtained with OPA pulse (654 nm, 29 nJ). Red dotted curve — spectrum obtained with a CW laser diode (658 nm, 100 μW). Inset shows that the two spectra coincide when the OPA pulse energy is very low (300 pJ). (b) Change of PL spectra with the pulse energy of OPA beam (654 nm) varied between 1 nJ and 30 nJ in the order of #1 to #7. Curve #4 corresponds to the highest fluence ($\sim 1.3 \times 10^{14}$ photons/cm²). (c) Change of PL spectra with the pulse energy of 653 nm light (FWHM = 10 nm) varied between 1 nJ and 20 nJ in the order of #1 to #7.

ure 1(b) shows PL spectra measured with pulse energies of 1 nJ (curves #1 and #7), 4 nJ (#2 and #6), 10 nJ (#3 and #5), and 30 nJ (#4). The (7,5) peak is dominant at low fluences while the (6,5) peak becomes dominant at high fluences. It is important to note that the different curves were taken in the order of #1 to #7, demonstrat-

ing that the observed changes are reproducible and are not caused by any laser-induced permanent change in the sample. Additionally, note that the PL intensities tend to saturate at high laser fluences, while their peak positions do not change at all.

Figure 1(c) shows PL spectra measured for the dried ι -carrageenan film using 653 nm optical pulses with a FWHM bandwidth of 10 nm at different pulse energies. The pulse energies were 1 nJ (curves #1 and #7), 3 nJ (#2 and #6), 10 nJ (#3 and #5), and 20 nJ (#4) measured in the order of #1 to #7. Figure 1(c) exhibits the same behavior as that shown in Fig. 1(b), demonstrating that the observed changes shown in Fig. 1(b) did not result from any artifacts, e.g., caused by the fluidic nature of the sample or by the unnoticed parasitic wavelength components in the OPA beam. In the following, we use the excitation pulse fluence in terms of the number of incident photons per cm^2 per pulse to express the intensity of excitation pulses.

Figures 2(a)-2(d) show PLE maps taken with various pump fluences. The step size for the pump photon energy was 20 meV. The data taken with the lowest fluence (1.2×10^{12} photons/ cm^2) [Fig. 2(a)] is essentially the same as that taken with low-intensity CW light. However, as the fluence is increased [Figs. 2(b)-2(d)], the E_{22} excitation peaks gradually broaden and eventually become completely flat at the highest fluence (1.2×10^{14} photons/ cm^2) — i.e., *PL intensities become independent of the excitation wavelength*. The corresponding PLE spectra are shown in Figs. 2(e)-2(h) for three PL wavelengths at 983, 1034, and 1125 nm. Again, such changes in the PLE spectra were reproducible over the fluence range tested here, indicating that no sample damage was induced.

In order to obtain PL intensity (I_{PL}) versus pump intensity (I_{pump}) relationships for different emission peaks, we measured PL spectra at different photon fluences for various excitation wavelengths. Each PL spectrum was decomposed and fitted by multiple peaks corresponding to the SWNT types/chiralities involved in the measured wavelength range. 50% Gaussian + 50% Lorentzian line-shape was assumed, and the decomposition was performed by optimizing the peak-width so that the decomposition gives the best fitting for the original PL spectrum. The optimum widths at the highest fluence was larger by $\sim 15\%$ than those at the lowest fluence in Fig. 1, and such an increment of the width is considered to be caused by the enhanced interactions among excitons or their reduced lifetime in the presence of high density excitons. Throughout the decomposition analysis performed, peak positions of all the PL features and the ratios among their widths were fixed regardless of the excitation wavelength and fluence.

Figure 3 shows the obtained integrated PL peak intensities (I_{PL}) plotted against the incident photon fluence (I_{pump}) for (6,5), (7,5), and (8,3) SWNTs at excitation wavelengths of 570, 615, and 658 nm. The resonance wavelengths of these SWNT types at the E_{22} levels are

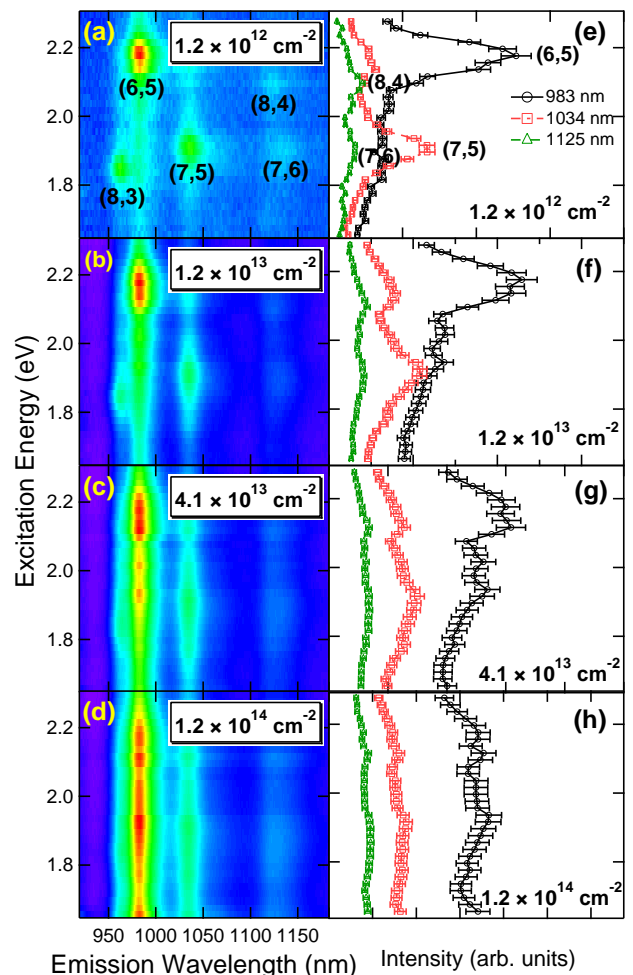


FIG. 2: (color online) Evolution of PLE data with increasing pump pulse fluence: (a) 1.2×10^{12} , (b) 1.2×10^{13} , (c) 4.1×10^{13} , and (d) 1.2×10^{14} photons/ cm^2 . (e-h): PLE spectra corresponding to (a)-(d) at emission wavelengths of 983 nm (circles), 1034 nm (squares), and 1125 nm (triangles).

approximately 570, 647, and 673 nm, respectively. It can be seen that the integrated PL intensity begins to saturate at a lower (higher) fluence when SWNTs are excited resonantly (non-resonantly). Unexpectedly fast saturation of the PL from (7,5) with 570 nm excitation (which is non-resonant) can be attributed to its proximity to the phonon sideband at ~ 585 nm.³⁴

C. Data interpretation

We interpret these observations as results of very efficient exciton-exciton annihilation,^{16,17,18,19,22,35} a non-radiative process that occurs at high exciton densities where two excitons are spatially close enough to interact with each other, resulting in the annihilation of the two excitons and simultaneous creation of an e - h pair in a higher energy state (either as a bound exciton or an un-

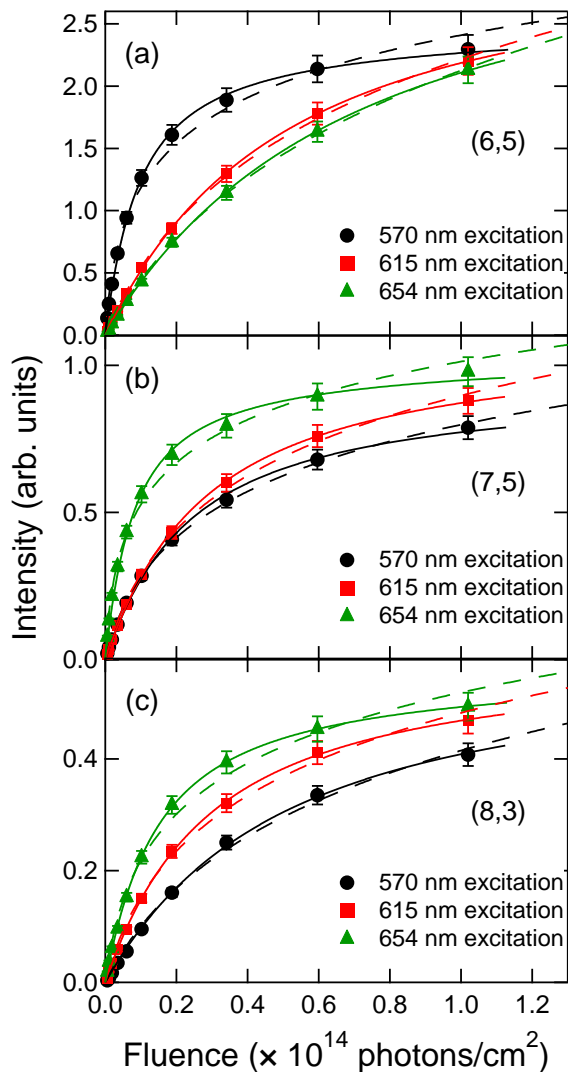


FIG. 3: (color online) Integrated PL intensity versus pump fluence for (6,5), (7,5), and (8,3) SWNTs. Pump wavelengths were 570 nm (circles), 615 nm (squares), and 654 nm (triangles). The error bars account for $\pm 5\%$. The solid and dashed curves are fitting by Eq. (15) and Eq. (20), respectively.

bound free e - h pair). We assume that the formation of E_{11} excitons occurs in a very short time scale after an optical excitation around E_{22} , because of much faster E_{22} -to- E_{11} relaxation (e.g., ~ 40 fs³⁶) than the duration of our OPA pulse (~ 250 fs). Thus, excitons quickly accumulate in the E_{11} state during and right after photo-creation of e - h pairs. However, the number of excitons that can be accommodated in the E_{11} state is limited by EEA. As the exciton density, n_x , approaches its maximum value, EEA begins to prevent a further increase by *efficiently removing excitons non-radiatively*, which explains the PL saturation behavior. Since EEA serves as a bottleneck for the exciton density, the PL intensity becomes insensitive to whether the excitons were created resonantly or non-resonantly around the E_{22} level and independent of

the pump wavelength, resulting in the flattening of PLE spectra. Namely, at very high pump fluences, the PL intensity is determined not by how efficiently excitons are created but by *how many E_{11} excitons can be accommodated within a particular type of SWNT* as well as by the relative abundance of that type of SWNT in the sample. We also performed optical transmission spectroscopy in the E_{22} range using OPA pulses and found that the absorption spectra do not exhibit any change even at high pulse fluences. Thus, nonlinear optical effects such as phase-space filling in the E_{22} range are not playing any role in the observed PLE broadening/flattening and PL saturation.

III. THEORY

In this section, we develop a theoretical model for explaining the experimental results, taking into account the generation, diffusion-limited EEA, and spontaneous decays of 1-D excitons. Under certain approximations, the model provides a direct analytical relationship between the intensity of the excitation light (I_{pump}) and that of the emitted PL (I_{PL}) for limiting cases, which allows us to estimate the density of excitons in SWNTs through fitting to the experimentally obtained I_{pump} vs. I_{PL} curves.

A. Model

Figure 4(a) shows a schematic energy diagram of the excitons in semiconducting SWNTs under consideration. We are interested in calculating the population of excitons N (indicated by the dotted box) in the lowest energy state E_{11} . First, excitons are created by optical excitation at an energy around the E_{22} level, which is typically in the visible wavelength range. The excitation intensity is denoted by I_{pump} . As soon as excitons are created, they decay to the E_{11} level within a very short time (~ 40 fs)³⁶ by transferring their energies to the lattice. Recent studies have reported that the excitons created around E_{22} levels primarily decay to the E_{11} level with a probability close to unity.^{37,38} The influx of excitons to the E_{11} level is denoted by G_{in} . On the other hand, the spontaneous decay time τ_{tot} of the E_{11} excitons to the ground state (G. S.) has been reported to be 10–100 ps.^{39,40,41} Such a spontaneous decay consists of radiative and non-radiative processes, with respective rates γ_r and γ_{nr} (s^{-1}), where $\gamma_r + \gamma_{\text{nr}} \equiv \gamma_{\text{tot}} = \tau_{\text{tot}}^{-1}$. The outflux of excitons from the E_{11} level *via the spontaneous decay process* is denoted by G_{out} . Therefore, the flux of the PL photons or the PL intensity (I_{PL}) is equal to ηG_{out} , where $\eta (\equiv \gamma_r / \gamma_{\text{tot}})$ denotes the branching ratio for the radiative decay from the E_{11} level.

As the density of excitons increases, the EEA process becomes important. If the e - h pair created in the higher energy state returns back to the E_{11} exciton level with a probability of λ ($0 \leq \lambda \leq 1$), the initial two excitons

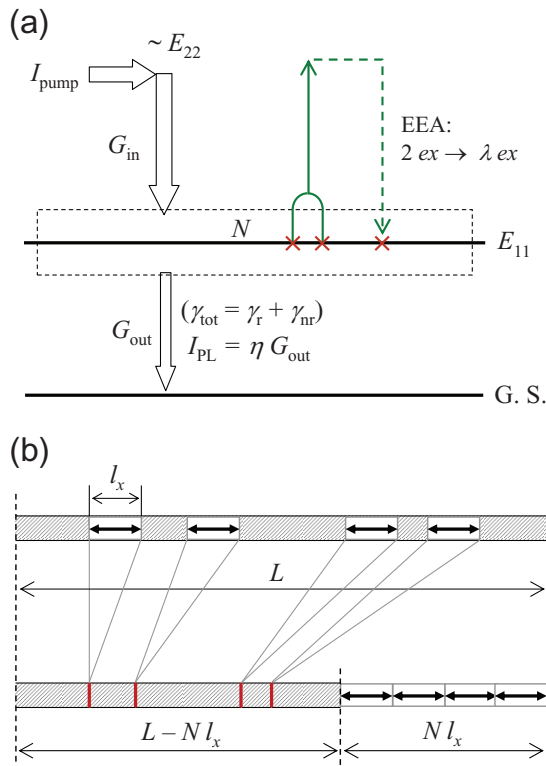


FIG. 4: (color online) (a) Schematic energy diagram of the system considered in the model. The dotted box enclosing the lowest energy level (E_{11}) is the domain of interest where N excitons are populated. All the symbols are defined in the text. (b) Schematic description of $N = 4$ excitons randomly distributed over a SWNT with a length of L . The horizontal arrow with a length of l_x denotes the average length traversed by one exciton during its spontaneous decay lifetime τ_{tot} . The lower part is the equivalent of the upper but emphasizes that the total length of the unoccupied region is $L - Nl_x$ where N vertical thick bars denote the borders of the areas occupied by those excitons. The ends of the SWNT are assumed to be a cyclic boundary.

are eventually reduced to λ excitons (as an expectation value) through such an EEA process. We make the following two assumptions: (1) Once two excitons intersect in a SWNT, EEA occurs instantaneously with a probability of one, and (2) the positions where excitons are created in SWNTs by optical excitations are random.

Figure 4(b) schematically shows a situation in which N excitons exist in a SWNT of length of L . Each exciton is considered to “occupy” a characteristic length l_x in a SWNT. In a static limit, l_x should simply be the exciton size. On the other hand, when exciton diffusion is present, l_x is assumed to be the average distance traveled by an exciton during the spontaneous decay lifetime τ_{tot} and is $\propto \sqrt{D\tau_{\text{tot}}}$, where D (cm^2/s) is the exciton diffusion constant. Namely, it is assumed that l_x is determined by the diffusion length, and any two excitons created within l_x undergo EEA.

First, a 1-D space of length L is considered where N

segments (or excitons) of length l_x are randomly present without overlapping each other, as shown in Fig. 4(b). The probability of a new segment (of length l_x) to enter the system *without* overlapping any of the N existing segments, $p(N)$, is given by the product of the following two probabilities

$$p_1 = 1 - \frac{Nl_x}{L} \quad (1)$$

which is the probability for the center of the new segment to land on an unoccupied area [hatched regions in Fig. 4(b)], and

$$p_2 = \left(1 - \frac{l_x}{L - Nl_x}\right)^N \quad (2)$$

which is the probability that the occupying length (l_x) of the new segment (whose center has landed on an unoccupied area) does not interfere with any of the N existing segments [vertical thick bars in the lower part of Fig. 4(b)]. Hence, $p(N)$ is written as

$$p(N) = \left(1 - \frac{Nl_x}{L}\right) \left(1 - \frac{l_x}{L - Nl_x}\right)^N. \quad (3)$$

The expectation value of the increment of N due to the introduction of a new segment into the system, $\langle \Delta N \rangle_N$ ($0 < \langle \Delta N \rangle_N \leq 1$), depends on the type of two-particle annihilation considered. For the general “ $ex + ex \rightarrow \lambda ex$ ” case, $\langle \Delta N \rangle_N$ is expressed as

$$\langle \Delta N \rangle_N = p(N) - (1 - \lambda)(1 - p(N)). \quad (4)$$

In the following, the derivation for the case of $\lambda = 1$ is shown as a specific example, since this case is considered to represent our experimental situation. The final results will be presented for both the $\lambda = 1$ and $\lambda = 0$ cases.

B. Solutions in limiting cases

1. Steady-state limit

Here, we consider the *steady-state* limit, where the number of excitons N in the system is steady, corresponding to CW excitation. In order to derive the relationship between I_{pump} and I_{PL} , we consider the relationship between G_{in} and G_{out} [see Fig. 4(a)], where both G_{in} and G_{out} are *rates*, having units of s^{-1} . When N is sufficiently small and EEA is negligible, $G_{\text{in}} = G_{\text{out}} = \gamma_{\text{tot}}N$. When EEA is present, however, this relationship becomes

$$G_{\text{in}} = \frac{G_{\text{out}}}{\langle \Delta N \rangle_N} = \frac{\gamma_{\text{tot}}N}{\langle \Delta N \rangle_N}. \quad (5)$$

In the case of $\lambda = 1$, Eq. (4) and Eq. (5) lead to

$$G_{\text{in}} = \frac{\gamma_{\text{tot}}N}{\left(1 - \frac{Nl_x}{L}\right) \left\{1 - \frac{l_x}{L} \left(1 - \frac{Nl_x}{L}\right)^{-1}\right\}^N}. \quad (6)$$

We introduce two dimensionless variables $\zeta \equiv Nl_x/L$ and $\psi \equiv G_{\text{in}}l_x/\gamma_{\text{tot}}L$, the former of which is a dimensionless exciton population ($0 \leq \zeta < 1$). Using these variables, Eq. (6) can then be rewritten in dimensionless form:

$$\psi = \frac{\zeta}{(1-\zeta) \left\{ 1 - \frac{l_x}{L}(1-\zeta)^{-1} \right\}^{\frac{l_x}{L}\zeta}}. \quad (7)$$

Expanding the second factor in the denominator of Eq. (7) and eliminating higher-order terms of l_x/L leads to an equation of only ζ and ψ , expressed as

$$\psi = \frac{\zeta}{(1-\zeta) \sum_{\kappa=0}^{\infty} \frac{(-1)^\kappa}{\kappa!} \left(\frac{\zeta}{1-\zeta} \right)^\kappa}. \quad (8)$$

Summing up to $\kappa = 6$ in Eq. (8) is sufficient to reproduce Eq. (7) for $l_x/L < 0.1$. Finally, noting that the denominator of Eq. (8) is equal to the Taylor expansion of an exponential function, the solution for the steady-state limit for $\lambda = 1$ ($ex + ex \rightarrow ex$) is expressed as

$$\psi = \frac{\zeta}{1-\zeta} \exp\left(\frac{\zeta}{1-\zeta}\right). \quad (9)$$

Here, since $I_{\text{PL}} \propto N$ and $I_{\text{pump}} \propto G_{\text{in}}$, I_{PL} and I_{pump} are proportional to ζ and ψ , respectively, i.e., $I_{\text{PL}} = c_1\zeta$ and $I_{\text{pump}} = c_2\psi$, where c_1 and c_2 are real constants.

On the other hand, the solution for the case of $\lambda = 0$ ($ex + ex \rightarrow 0$) is derived through a similar procedure, yielding

$$\psi = \frac{\zeta}{2(1-\zeta)\exp\left(-\frac{\zeta}{1-\zeta}\right) - 1}. \quad (10)$$

Equations (9) and (10), valid for CW PL experiments, are implicit equations relating the PL intensity (I_{PL}) and the pump intensity (I_{pump}) in terms of their respective dimensionless variables ζ and ψ . These equations contain no fitting parameters except the two linear scaling factors c_1 and c_2 and simply become equivalent ($\zeta = \psi$) in the low density limit ($\zeta \rightarrow 0$).

2. Instantaneous limit

Here, we consider the *instantaneous* limit in which creation of all the excitons by an infinitesimally short optical pulse and their internal relaxation to E_{11} level occur instantaneously at $t = 0$, before diffusion-limited EEA and spontaneous decay processes begin to occur subsequently. This limit represents a situation where the duration of the optical pulse and the time required for intraband relaxation are much shorter than the spontaneous decay time τ_{tot} , as in the case of the present experimental situation. The pump intensity I_{pump} in this limit is directly proportional to N_0 , the number of excitons or e - h pairs

created at $t = 0$, while the PL intensity I_{PL} is proportional to the number of excitons N that survived EEA. The relationship between N_0 and N is described by the differential equation

$$dN_0 = \frac{dN}{\langle \Delta N \rangle_N} \quad (11)$$

where $\langle \Delta N \rangle_N$ is given by Eq. (4). When $\lambda = 1$ is assumed, Eq. (11) is rewritten as

$$\frac{dN_0}{dN} = \frac{1}{\left(1 - \frac{Nl_x}{L}\right) \left\{ 1 - \frac{l_x}{L} \left(1 - \frac{Nl_x}{L}\right)^{-1} \right\}^N}. \quad (12)$$

As in the previous case (steady-state limit), we introduce dimensionless variables $\zeta \equiv Nl_x/L$ and $\psi \equiv N_0l_x/L$. Again, since $I_{\text{PL}} \propto N$ and $I_{\text{pump}} \propto N_0$, $I_{\text{PL}} = c_1\zeta$ and $I_{\text{pump}} = c_2\psi$, where c_1 and c_2 are constants. With ζ and ψ , Eq. (12) can be written in a dimensionless form:

$$\frac{d\psi}{d\zeta} = \frac{1}{(1-\zeta) \left\{ 1 - \frac{l_x}{L}(1-\zeta)^{-1} \right\}^{\frac{l_x}{L}\zeta}}. \quad (13)$$

Furthermore, similar to the steady-state case, an expansion is performed on the second factor in the denominator of Eq. (13) together with elimination of the higher-order terms of l_x/L , resulting in a differential equation of only ζ and ψ :

$$\frac{d\psi}{d\zeta} = \frac{1}{1-\zeta} \exp\left(\frac{\zeta}{1-\zeta}\right). \quad (14)$$

Finally, by integrating Eq. (14) from 0 to ζ , we obtain the solution for $\lambda = 1$ ($ex + ex \rightarrow ex$) as

$$\psi = \frac{1}{e} \left\{ \text{Ei}\left(\frac{1}{1-\zeta}\right) - \text{Ei}(1) \right\}, \quad (15)$$

where

$$\text{Ei}(x) = \int_{-\infty}^x \frac{e^y}{y} dy \quad (16)$$

is the exponential integral.

Similarly, the solution for $\lambda = 0$ ($ex + ex \rightarrow 0$) in the instantaneous limit is

$$\psi = \int_0^\zeta \frac{1}{2(1-\zeta)\exp\left(-\frac{1}{1-\zeta}\right) - 1} d\zeta \quad (17)$$

where the integral has to be solved numerically. Those dimensionless equations (15) and (17) become equivalent ($\zeta = \psi$) in the low density limit ($\zeta \rightarrow 0$).

IV. COMPARISONS AND DISCUSSION

A. Comparison of model and experiment

To compare with the experimental data shown in Fig. 3, we use Eq. (15), which is for the instantaneous

limit with $\lambda = 1$. The choice of this equation is because of the short duration of the optical pulses used (~ 250 fs), the very fast (~ 40 fs³⁶) and efficient^{37,38} internal decay of excitons created at E_{22} levels to the lowest E_{11} level, and the much longer spontaneous decay time from the E_{11} level to G. S. (10–100 ps).^{39,40,41} The solid curves shown in Fig. 3 are fitting curves using Eq. (15), indicating that the model agrees well with the experimentally observed PL saturation curves.

Table I is a summary of the fitting analysis performed on the data in Fig. 3 using Eq. (15). The first two columns show the optimum values of the scaling factors c_1 and c_2^{-1} . These are thought to be proportional to the oscillator strength for the PL emission from E_{11} levels and the oscillator strength for the optical absorption around E_{22} levels, respectively, as expected from $I_{\text{PL}} \propto c_1 N$ and $N_0 \propto c_2^{-1} I_{\text{pump}}$. The right three columns (ζ , N , and R) are values at 1.02×10^{14} photons/cm² (see Fig. 3). The values of N were obtained through the relationship $N = \zeta/l_x$, where l_x was assumed to be 45 nm (one half of the average exciton excursion range defined in Ref. 31). The exciton density in the highly saturated regime ($\sim 1 \times 10^5$ cm⁻¹) is still more than one order magnitude smaller than the expected Mott density in SWNTs ($\sim 7 \times 10^6$ cm⁻¹, assuming an exciton size of ~ 1.5 nm⁴²), as has been discussed in detail in Ref. 32. R in the right-most column denotes the ratio between the number of as-created e - h pairs and the number of excitons that survived the EEA process until their spontaneous decay to G. S., or N_0/N . The values of R show that approximately 90% of the initially created e - h pairs/excitons decay non-radiatively through the EEA path when the E_{22} levels are resonantly excited at a fluence of 1.02×10^{14} photons/cm².

As expected, the values of c_1 are similar within the same chirality type, regardless of the excitation wavelength. However, for the particular case of (6,5) with 570 nm excitation, where the excitation wavelength exactly coincided with the E_{22} resonance peak, the value of c_1 ($\sim 3 \times 10^5$) is appreciably smaller than those at the other excitation wavelengths ($\sim 4 \times 10^5$). Such a smaller c_1 value implies that more excitons decayed to the G. S. through non-radiative paths compared to the other cases. This may be due to an emergence of stronger nonlinear processes that have not been taken into account in the assumptions, such as the breakdown of the $\lambda = 1$ assumption and/or the appearance of *more-than-two*-body annihilation processes because of the very high initial e - h pair density, achieved with the strong E_{22} resonance in this particular case.

The values of c_2^{-1} also show the expected tendency toward higher (lower) values when the excitation wavelength is closer to (further from) the E_{22} resonance wavelength. The slightly higher c_2^{-1} value for the case of (7,5) with 570 nm excitation is again attributed to its vicinity to the E_{22} phonon sideband at ~ 585 nm.³⁴

Type	Exct. (nm)	c_1 ($\times 10^5$)	c_2^{-1} ($\times 10^{-14}$)	ζ	N ($\times 10^5$ cm ⁻¹)	R
(6,5)	570	2.97	7.74	0.764	1.70	10.3
	615	3.89	1.54	0.566	1.26	2.78
	654	4.21	1.13	0.505	1.12	2.28
(7,5)	570	1.14	3.18	0.678	1.51	4.77
	615	1.34	2.68	0.656	1.46	4.17
	654	1.22	9.16	0.776	1.72	12.0
(8,3)	570	0.73	1.54	0.566	1.26	2.78
	615	0.72	2.61	0.652	1.45	4.07
	654	0.68	5.05	0.729	1.62	7.05

TABLE I: Summary of the optimal parameters to used fit the experimental data, obtained from the analysis with Eq. (15). ζ , N , and R are values at the fluence of 1.02×10^{14} photons/cm², corresponding to the largest fluence in Fig. 3.

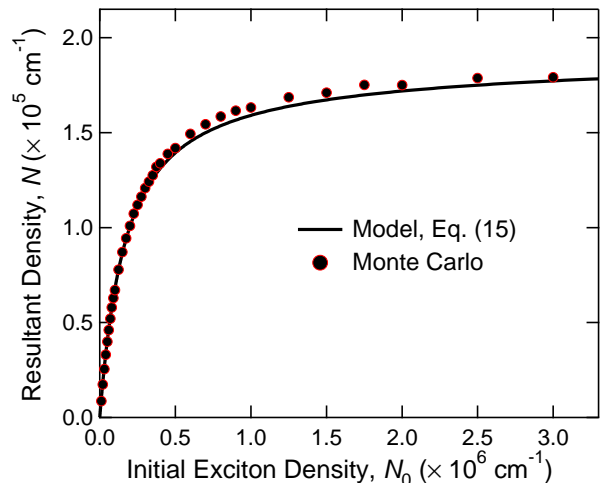


FIG. 5: (color online). Comparison between the saturation behavior predicted by Eq. (15) (black solid curve) and the result obtained by a Monte Carlo simulation of the EEA process. The abscissa denotes the density of initially created excitons while the ordinate corresponds to the resultant density. The experimental range of N_0 in Fig. 3 is $N_0 \leq 2 \times 10^6$ cm⁻¹.

B. Comparison with Monte Carlo calculation

To further confirm the validity of the model, we performed a computational simulation based on the Monte Carlo method. At the beginning of the simulation, a random distribution of N_0 excitons along a line is created at time $t = 0$, corresponding to the instantaneous limit. For $t > 0$, each exciton undergoes a random movement in each computational step dt by the distance given by the probability distribution of $\bar{N}(0, l_0^2)$, where $\bar{N}(x_0, \sigma^2)$ denotes the normal distribution centered at x_0 with variance σ and $l_0 \equiv \sqrt{Ddt}$. Upon intersection of any two excitons, the EEA of $\{ex + ex \rightarrow ex\}$ takes place. In addition, each exciton is eliminated from the system with a probability of $\gamma_{\text{tot}} dt$ ($= \tau_{\text{tot}}^{-1} dt$), corresponding to possible spontaneous decay during each computational step.

The total density of excitons that have decayed spontaneously (N) can thus be calculated for each value of the initial density N_0 .

Figure 5 shows a comparison between the model for the instantaneous limit [Eq. (15)] with $l_x = 45$ nm and the result of the Monte Carlo simulation, plotting the relationship of N_0 and N . The simulation was performed with $D = 0.42$ cm²/s and $\tau_{\text{tot}} = 100$ ps,⁴³ which resulted in an average exciton displacement of 45 nm based on the same simulation performed without EEA. The comparison shows satisfactory agreement, indicating that the simple analytical form of Eq. (15) well describes the phenomenon of diffusion-limited EEA, hence validating our model.

C. Comparison with conventional rate-equation solution

Conventionally, a rate equation of the form

$$\frac{dN(t)}{dt} = G_{\text{in}}(t) - \gamma_{\text{tot}}N(t) - \gamma_{\text{EEA}}N(t)^2 \quad (18)$$

has been used to explain EEA processes observed for various materials from 1-D to 3-D.^{17,18,19,22,44,45,46} The terms on the right hand side, from left to right, represent the rate of excitons entering the system (or the E_{11} level in the present case), the rate of excitons spontaneously decaying from the system to the G. S. (at γ_{tot}), and the rate of excitons leaving the system because of EEA (at γ_{EEA}), respectively. Here, the probability of finding two excitons at the same position (or the EEA rate) is assumed to be proportional to N^2 , and hence, exciton diffusion as well as the finite size (i.e., length) that each 1-D exciton occupies are not taken into account in Eq. (18).

Equation (18) is solved for the pulse-wise creation of N_0 excitons at $t = 0$ [i.e., $G_{\text{in}}(t) = \delta(N_0)$] in order to be compared with the proposed model for the instantaneous limit [Eq. (15)] as well as with the experimental results. With this initial condition, Eq. (18) is readily solved to be

$$N(t) = \frac{1}{\left(\frac{1}{N_0} + \Gamma\right) \exp(\gamma_{\text{tot}}t) - \Gamma} \left[\Gamma \equiv \frac{\gamma_{\text{EEA}}}{\gamma_{\text{tot}}} \right]. \quad (19)$$

The total number of photons emitted from the sample, I_{PL} , is obtained by integrating Eq. (19) from $t = 0$ to ∞ as

$$I_{\text{PL}} = \eta \int_0^{\infty} \gamma_{\text{tot}}N(t)dt = -\frac{\eta}{\Gamma} \ln \left\{ 1 - \left(1 + \frac{1}{N_0\Gamma} \right)^{-1} \right\} \quad (20)$$

where $\eta = \gamma_r/\gamma_{\text{tot}}$ as before. Equation (20) describes the relationship between I_{PL} and N_0 in terms of two adjustable components η/Γ and $N_0\Gamma$.

The dashed lines drawn in Fig. 3 are the optimum fits by Eq. (20) to the experimental data. While Eq. (20) reproduces the behavior well for the regime of weaker PL

saturation with non-resonant excitations, the deviation becomes clearer for the regime of stronger PL saturation with resonant excitations. Most importantly, however, the density predicted by Eq. (20) has *no upper limit* as recognized by the steadily increasing dashed lines shown in Fig. 3 [or by the logarithmic form of Eq. (20)], while Eq. (15) correctly demonstrates the existence of an upper limit, as observed experimentally and in the Monte Carlo simulation.

Another important difference between Eq. (15) and Eq. (20) is described as follows: The solution of the conventional rate equation [Eq. (20)] contains two independent quantities: η/Γ and $N_0\Gamma$. The former can be used to scale I_{PL} . However, since the parameter $N_0\Gamma$ simultaneously scales $I_{\text{pump}} (\propto N_0)$ and changes the shape of the saturation curve, one essentially cannot estimate the density of excitons from the fitting analysis based on Eq. (20). On the other hand, since the shape of Eq. (15) has been uniquely determined by its dimensionless representation, the only thing one can do is to *linearly and independently* change the two scaling constants c_1 and c_2 for I_{PL} and I_{pump} , respectively, yielding sets of ζ and ψ values along the scaled (or fitted) I_{PL} vs. I_{pump} curves.

V. SUMMARY

We have investigated photoemission properties of high-density 1-D excitons in single-walled carbon nanotubes. As the excitation intensity increases, all photoluminescence emission peaks arising from different chiralities showed clear saturation in intensity. Each peak exhibited a saturation value that was independent of the excitation wavelength, indicating that there is an upper limit on the exciton density for each nanotube species. We interpret these results in terms of diffusion-limited exciton-exciton annihilation processes through which high-density excitons decay non-radiatively.

To quantitatively understand the saturation behavior observed in the experiment, we have developed a theoretical model, taking into account the generation, diffusion-limited exciton-exciton annihilation, and spontaneous decays of 1-D excitons. The saturation curve predicted by the model under appropriate approximations reproduced the experimental saturation curves well, and the fitting analysis allowed us to estimate the density of excitons for a given diffusion constant. We also compared our results with Monte Carlo calculations, confirming the validity of our model. Additionally, we examined the saturation behavior predicted by the solution of the conventional exciton-exciton annihilation rate equation that does not take into account diffusion and showed that the solution qualitatively failed to fit the experimental data at high exciton densities, showing the inappropriateness of its use for excitons in carbon nanotubes. The approach presented in this paper should have wide applicability for predicting the intensities of photoluminescence from single-walled carbon nanotubes under various excitation

conditions.

An important conclusion drawn from the current study is that a large density of electron-hole pairs is difficult to achieve in single-walled carbon nanotubes. This imposes a serious challenge for making active optoelectronic devices based on semiconducting single-walled carbon nanotubes — 1-D semiconductor lasers, in particular, which would require densities comparable to, or higher than, the Mott density. The existence of an upper limit on the density of excitons would also prevent fundamental studies of bosonic characters of 1-D excitons expected at quantum-degenerate densities. Hence, novel methods are needed for minimizing non-radiative decay processes such as exciton-exciton annihilation in single-walled carbon nanotubes, which would require ways to control the dynamic parameters of excitons such as the spontaneous decay rate and diffusion constant through, e.g., varying

the temperature as well as applying an external magnetic field.⁴⁷

Acknowledgments

The authors thank Ajit Srivastava for valuable discussions and Erik Einarsson for emendation. We thank the Robert A. Welch Foundation (C-1509) and NSF (DMR-0325474 and OISE-0530220) for support. One of us (Y. M.) was financially supported by Grants-in-Aid for Scientific Research (#18-09883) from the Japan Society for the Promotion of Science (JSPS). Y. M. thanks Tatsuya Okubo and Shigeo Maruyama for support to his fulfillment of the JSPS research program.

-
- * ymurak@chemsys.t.u-tokyo.ac.jp; corresponding author.
- ¹ T. Ogawa and Y. Kanemitsu, eds., *Optical Properties of Low-Dimensional Materials* (World Scientific Publishing Co., Singapore, 1995).
 - ² T. Giamarchi, *Quantum Physics in One Dimension* (Oxford University Press, New York, 2004).
 - ³ R. S. Knox, *Theory of Excitons* (Academic Press, New York, 1963).
 - ⁴ T. Ogawa and T. Takagahara, Phys. Rev. B **43**, 14325 (1991); **44**, 8138 (1991).
 - ⁵ F. Rossi and E. Molinari, Phys. Rev. Lett. **76**, 3642 (1996).
 - ⁶ E. Kapon, D. M. Hwang, and R. Bhat, Phys. Rev. Lett. **63**, 430 (1989).
 - ⁷ W. Wegscheider, L. N. Pfeiffer, M. M. Dignam, A. Pinczuk, K. W. West, S. L. McCall, and R. Hull, Phys. Rev. Lett. **71**, 4071 (1993).
 - ⁸ R. Ambigapathy, I. Bar-Joseph, D. Y. Oberli, S. Haacke, M. J. Brasil, F. Reinhardt, E. Kapon, and B. Deveaud, Phys. Rev. Lett. **78**, 3579 (1997).
 - ⁹ S. Das Sarma and D. W. Wang, Phys. Rev. Lett. **84**, 2010 (2000).
 - ¹⁰ D. W. Wang and S. Das Sarma, Phys. Rev. B **64**, 195313 (2001).
 - ¹¹ J. Rubio, L. Pfeiffer, M. H. Szymanska, A. Pinczuk, S. He, H. U. Baranger, P. B. Littlewood, K. W. West, and B. S. Dennis, Solid State Commun. **120**, 423 (2001).
 - ¹² H. Akiyama, L. N. Pfeiffer, M. Yoshita, A. Pinczuk, P. B. Littlewood, K. W. West, M. J. Matthews, and J. Wynn, Phys. Rev. B **67**, 041302 (2003).
 - ¹³ T. Guillet, R. Grousson, V. Voliotis, M. Menant, X. L. Wang, and M. Ogura, Phys. Rev. B **67**, 235324 (2003).
 - ¹⁴ M. Yoshita, Y. Hayamizu, H. Akiyama, L. N. Pfeiffer, and K. W. West, Phys. Rev. B **74**, 165332 (2006).
 - ¹⁵ Y. Hayamizu, M. Yoshita, Y. Takahashi, H. Akiyama, C. Z. Ning, L. N. Pfeiffer, and K. W. West, Phys. Rev. Lett. **99**, 167403 (2007).
 - ¹⁶ Q.-H. Xu, D. Moses, and A. J. Heeger, Phys. Rev. B **68**, 174303 (2003).
 - ¹⁷ G. Dicker, M. P. de Haas, and L. D. A. Siebbeles, Phys. Rev. B **71**, 155204 (2005).
 - ¹⁸ Y. Zaushitsyn, K. G. Jespersen, L. Valkunas, V. Sundstrom, and A. Yartsev, Phys. Rev. B **75**, 195201 (2007).
 - ¹⁹ S. M. King, D. Dai, C. Rothe, and A. P. Monkman, Phys. Rev. B **76**, 085204 (2007).
 - ²⁰ F. Wang, G. Dukovic, E. Knoesel, L. E. Brus, and T. F. Heinz, Phys. Rev. B **70**, 241403 (2004).
 - ²¹ G. N. Ostojic, S. Zaric, J. Kono, V. C. Moore, R. H. Hauge, and R. E. Smalley, Phys. Rev. Lett. **94**, 097401 (2005).
 - ²² Y.-Z. Ma, L. Valkunas, S. L. Dexheimer, S. M. Bachilo, and G. R. Fleming, Phys. Rev. Lett. **94**, 157402 (2005).
 - ²³ S. Iijima and T. Ichihashi, Nature **363**, 603 (1993).
 - ²⁴ A. Jorio, G. Dresselhaus, and M. Dresselhaus, eds., *Carbon Nanotubes: Advanced Topics in the Synthesis, Structure, Properties and Applications* (Springer, Berlin, 2008).
 - ²⁵ C. D. Spataru, S. Ismail-Beigi, L. X. Benedict, and S. G. Louie, Phys. Rev. Lett. **92**, 077402 (2004).
 - ²⁶ F. Wang, G. Dukovic, L. E. Brus, and T. F. Heinz, Science **308**, 838 (2005).
 - ²⁷ J. Maultzsch, R. Pomraenke, S. Reich, E. Chang, D. Prezzi, A. Ruini, E. Molinari, M. S. Strano, C. Thomsen, and C. Lienau, Phys. Rev. B **72**, 241402 (2005).
 - ²⁸ D. Moses, J. Wang, A. J. Heeger, N. Kirova, and S. Brazovskii, Proc. Natl. Acad. Sci. **98**, 13496 (2001).
 - ²⁹ C.-X. Sheng, Z. V. Vardeny, A. B. Dalton, and R. H. Baughman, Phys. Rev. B **71**, 125427 (2005).
 - ³⁰ R. M. Russo, E. J. Mele, C. L. Kane, I. V. Rubtsov, M. J. Therien, and D. E. Luzzi, Phys. Rev. B **74**, 041405 (2006).
 - ³¹ L. Cagnet, D. A. Tsybouski, J. R. Rocha, C. D. Donlye, J. M. Tour, and R. B. Weisman, Science **316**, 1465 (2007).
 - ³² Y. Murakami and J. Kono, Phys. Rev. Lett., in press. See also, arXiv:0804.3190v1.
 - ³³ Y. Tan and D. E. Resasco, J. Phys. Chem. B **109**, 14454 (2005).
 - ³⁴ Y. Miyauchi and S. Mauryama, Phys. Rev. B **74**, 035415 (2006).
 - ³⁵ A. Suna, Phys. Rev. B **1**, 1716 (1970).
 - ³⁶ C. Manzonni, A. Gambetta, E. Menna, M. Meneghetti, G. Lanzani, and G. Cerullo, Phys. Rev. Lett. **94**, 207401 (2005).
 - ³⁷ T. Hertel, V. Perebeinos, J. Crochet, K. Arnold, M. Kappes, and P. Avouris, Nano Lett. **8**, 87 (2008).
 - ³⁸ S. Lebedkin, F. Henrich, O. Kiowski, and M. M. Kappes,

- Phys. Rev. B **77**, 165429 (2008).
- ³⁹ G. N. Ostojic, S. Zaric, J. Kono, M. S. Strano, V. C. Moore, R. H. Hauge, and R. E. Smalley, Phys. Rev. Lett. **92**, 117402 (2004).
- ⁴⁰ F. Wang, G. Dukovic, L. E. Brus, and T. F. Heinz, Phys. Rev. Lett. **92**, 177401 (2004).
- ⁴¹ S. Reich, M. Dworzak, A. Hoffmann, C. Thomsen, and M. S. Strano, Phys. Rev. B **71**, 033402 (2005).
- ⁴² V. Perebeinos, J. Tersoff, and P. Avouris, Phys. Rev. Lett. **92**, 257402 (2004).
- ⁴³ The choice of these D and τ_{tot} values for the simulation is based on Ref. 31, in which $D \sim 0.4 \text{ cm}^2/\text{s}$ was derived from the experimentally determined “average exciton excursion range” (Λ) of 90 nm assuming $\tau_{\text{tot}} = 100$ ps. The l_x value used for the present model is half of Λ , based on the definition of Λ in Ref. 31.
- ⁴⁴ L. Valkunas, G. Trinkunas, V. Liuolia, and G. Grondelle, Biophys. J. **69**, 1117 (1995).
- ⁴⁵ T. W. Roberti, N. J. Cherepy, and J. Z. Zhang, J. Chem. Phys. **108**, 2143 (1998).
- ⁴⁶ K. E. O’Hara, L. O. Suilleabhain, and J. P. Wolfe, Phys. Rev. B **60**, 10565 (1999).
- ⁴⁷ A. Srivastava and J. Kono, arXiv:0810.5748v1.